
















Article

Radiobiological Outcomes, Microdosimetric Evaluations and Monte Carlo Predictions in Eye Proton Therapy

Giada Petringa^{1,2,†}, Marco Calvaruso^{1,3,*}, Valeria Conte⁴, Pavel Bláha⁵, Valentina Bravatà^{1,3}, Francesco Paolo Cammarata^{1,3}, Giacomo Cuttone^{1,6}, Giusi Irma Forte^{1,3}, Otilija Keta⁷, Lorenzo Manti^{5,8}, Luigi Minafra^{1,3}, Vladana Petković⁷, Ivan Petrović⁷, Selene Richiusa^{1,3}, Aleksandra Ristić Fira⁷, Giorgio Russo^{1,3} and Giuseppe Antonio Pablo Cirrone^{1,6,9,†}

- ¹ Istituto Nazionale di Fisica Nucleare-Laboratori Nazionali del Sud, 95125 Catania, Italy; giada.petringa@lns.infn.it (G.P.); valentina.bravata@ibfm.cnr.it (V.B.); francesco.cammarata@ibfm.cnr.it (F.P.C.); cuttone@lns.infn.it (G.C.); giusi.forte@ibfm.cnr.it (G.I.F.); luigi.minafra@ibfm.cnr.it (L.M.); selly_93r@hotmail.it (S.R.); giorgio.russo@ibfm.cnr.it (G.R.); pablo.cirrone@infn.it (G.A.P.C.)
- ² Extreme Light Infrastructure (ELI)-Beamlines Center, Institute of Physics (FZU), Czech Academy of Sciences, 117 20 Prague, Czech Republic
- ³ Istituto di Bioimmagini e Fisiologia Molecolare-Consiglio Nazionale delle Ricerche (IBFM-CNR), 90015 Cefalù, Italy
- ⁴ Istituto Nazionale di Fisica Nucleare-Laboratori Nazionali di Legnaro, INFN, 35020 Legnaro, Italy; valeria.conte@lnl.infn.it
- ⁵ Istituto Nazionale di Fisica Nucleare, Sezione di Napoli, 80126 Napoli, Italy; pavel.blahax@gmail.com (P.B.); lorenzo.manti@na.infn.it (L.M.)
- ⁶ Dipartimento di Fisica ed Astronomia “E.Majorana”, Catania University, 95124 Catania, Italy
- ⁷ Vinča Institute of Nuclear Sciences, University of Belgrade, 11000 Belgrade, Serbia; otilijak@vin.bg.ac.rs (O.K.); vladana@vin.bg.ac.rs (V.P.); ipetrov@vin.bg.ac.rs (I.P.); aristic@vin.bg.ac.rs (A.R.F.)
- ⁸ Dipartimento di Fisica “E. Pancini”, Radiation Biophysics Laboratory, Università Federico II di Napoli, 80126 Napoli, Italy
- ⁹ Centro Siciliano di Fisica Nucleare e Struttura della Materia, 95123 Catania, Italy
- * Correspondence: marco.calvaruso@ibfm.cnr.it
- † These authors contributed equally to this work.



Citation: Petringa, G.; Calvaruso, M.; Conte, V.; Bláha, P.; Bravatà, V.; Cammarata, F.P.; Cuttone, G.; Forte, G.I.; Keta, O.; Manti, L.; et al. Radiobiological Outcomes, Microdosimetric Evaluations and Monte Carlo Predictions in Eye Proton Therapy. *Appl. Sci.* **2021**, *11*, 8822. <https://doi.org/10.3390/app11198822>

Academic Editors: Ivan Veronese and Salvatore Gallo

Received: 14 July 2021

Accepted: 18 September 2021

Published: 23 September 2021

Publisher’s Note: MDPI stays neutral with regard to jurisdictional claims in published maps and institutional affiliations.



Copyright: © 2021 by the authors. Licensee MDPI, Basel, Switzerland. This article is an open access article distributed under the terms and conditions of the Creative Commons Attribution (CC BY) license (<https://creativecommons.org/licenses/by/4.0/>).

Abstract: CATANA (Centro di AdroTerapia ed Applicazioni Nucleari Avanzate) was the first Italian protontherapy facility dedicated to the treatment of ocular neoplastic pathologies. It is in operation at the LNS Laboratories of the Italian Institute for Nuclear Physics (INFN-LNS) and to date, 500 patients have been successfully treated. Even though proton therapy has demonstrated success in clinical settings, there is still a need for more accurate models because they are crucial for the estimation of clinically relevant RBE values. Since RBE can vary depending on several physical and biological parameters, there is a clear need for more experimental data to generate predictions. Establishing a database of cell survival experiments is therefore useful to accurately predict the effects of irradiations on both cancerous and normal tissue. The main aim of this work was to compare RBE values obtained from in-vitro experimental data with predictions made by the LEM II (Local Effect Model), Monte Carlo approaches, and semi-empirical models based on LET experimental measurements. For this purpose, the 92.1 uveal melanoma and ARPE-19 cells derived from normal retinal pigmented epithelium were selected and irradiated in the middle of clinical SOBP of the CATANA proton therapy facility. The remarkable results show the potentiality of using microdosimetric spectrum, Monte Carlo simulations and LEM model to predict not only the RBE but also the survival curves.

Keywords: protontherapy; proton; RBE; radiobiology; microdosimetry; Geant4

1. Introduction

Proton beam therapy is becoming increasingly available due to its potential to deliver maximal doses on tumour while minimizing irradiation of surrounding healthy

tissues/organs at risk. In fact, its ballistic precision has always been regarded as the main physical pillars of such a treatment modality [1]. However, in recent years, with growing numbers of patients treated and longer follow-up periods, concerns about the potential side effects of protontherapy have arisen [2,3]. The potential of a given particle irradiation to induce a greater level of specific biological effects compared to photon irradiation, used as a reference, is expressed in terms of its Relative Biological Effectiveness (RBE) [2]. Nowadays, in the proton-therapy clinical practice, a fixed RBE of 1.1 is assumed [3–5]. This reflects the known relationship between RBE and Linear Energy Transfer (LET), as in the tumour volume low-LET protons can be generally found. Despite this, data emerging from various radiobiological studies indicate that RBE of protons exceed the accepted value, at least in the distal part of the clinical spread out dose distribution, where high-LET slowing-down protons become predominant. Hence, a variable RBE should be used to more precisely describe the radiobiological effects on the tissues and organs involved in the treatment [6–10].

Successful treatment planning largely depends on the accuracy of biophysical models. To assure their precision they need to be validated against data from *in vitro* studies. Therefore, development of the database with experimental results obtained on various cell lines is useful for RBE model validation as well as for comparing different models [11].

While a vast literature exists reporting on the clinical results of eye proton therapy [12–16], no *in vitro* data evaluating the cellular radioresponse of uveal cancer cells along a clinical proton SOBPs are available. There is only scarce data regarding the response of human melanoma cell lines along with the proton spread-out Bragg peak. According to these data, at the distal end of a 65 MeV proton SOBPs, an RBE of 1.27 and even higher for the more resistant melanoma cell lines were recorded [17–19]. More recently, work carried out on uveal melanoma Mel270 cells at the mid-SOBPs position of a clinical high-energy proton beam showed an increased anti-migratory effect compared to photon irradiation [20]. Currently, many commercial Treatment Planning Systems (TPSs) for proton therapy incorporate the capability of calculating LET distributions and RBE estimations, but there remain challenges on how to deal with uncertainties resulting from potential RBE variations. Future TPS that would potentially be able to take into account RBE variability, could reduce the toxicity and the incidence of later-occurring induced morbidities, thus making it possible to exploit the full potential of proton therapy [2]. The main aim of this work was to study the RBE values at the clinical SOBPs of the CATANA proton therapy facility. Radiation-induced biological effects measured in terms of clonogenic cell death (see below) were predicted by the LEM II (Local Effect Model) [21], Monte Carlo approaches [22], and semi-empirical models based on LET experimental measurements [23]. All adopted methods were then compared with *in-vitro* experimental results. These were evaluated using the human 92.1 uveal melanoma cell line, a well-known model to investigate the aggressive behaviour of such types of neoplasia. In order to compare the effects induced by proton therapy in a non-tumorigenic cell line the human normal retinal pigment epithelial ARPE-19 cell line was also irradiated. The normal cells can easily recover from damage induced by ionizing radiation due to a more efficient damage response machinery with respect to the cancer cells. Moreover, choosing the normal retinal pigment epithelial ARPE-19 cell line allows obtaining insights into the magnitude of biological effects induced by an erroneous dose distribution during a proton therapy treatment plan. The retina is the organ at risk in uveal melanoma treatment and despite the usually excellent precision granted by protontherapy, the anatomical structure of the eye, with dimensions in the order of the millimeter is such that lack of a rigorous dose contouring is possible in actual clinical scenarios, leading to unwanted dose deposition. Such information is therefore of paramount importance to provide an estimate of the possible adverse effects deriving by beam forward straggling. Microdosimetry experimental spectra acquired to estimate the proton LET in different positions along the SOBPs, were measured in the same experimental conditions of the biological sample irradiation. Two different detectors were used to this scope: a mini-TEPC [24,25], developed at the Legnaro National Laboratories of the National Institute

for Nuclear Physics (LNL-INFN) and a Silicon On Insulator (SOI) microdosimeter with 3D Sensitive Volumes (MicroPlus-Bridge) [26,27]. The Loncol's weighting function was then applied to assess the microdosimetric RBE and compare it with the experimental one. The biological damage was estimated also adopting a computational method which couples Geant4 with the LEM-II model as well as the pure LEM-II model. In such a way, it was possible to compare the well-established LEM with a Monte Carlo method and a semi-empirical one and to establish an approach that best reproduces the biological data at a depth of 24 mm, the mid-position of the spread-out Bragg peak.

2. Material and Methods

2.1. CATANA Proton Therapy Facility

The CATANA protontherapy facility [28], built thanks to a collaboration between INFN-LNS and University of Catania Hospital "AOU-Vittorio Emanuele" in Catania (I), has been active since 2002 and successfully treated more than 500 patients. CATANA is dedicated to the radiation treatment of ocular melanomas with the 62 MeV proton beams accelerated by the INFN-LNS superconducting cyclotron. The most frequent neoplasia treated with proton beams is the uveal melanoma, followed by other eye diseases like choroidal metastases, conjunctival tumours, and eyelid tumours. The CATANA facility is based on a passive transport system. The proton maximal range, at the irradiation point, is about 30 mm, ideal for the treatment of eye tumours. The necessary maximum range and energy modulation are achieved by means of a set of polymethyl-methacrylate (or PMMA) absorbers, variable in thickness, and modulator wheels.

2.2. Experimental Set-Up

The clinical SOBP beam configuration was used for the radiobiological and microdosimetric measures. The SOBP penetration range, measured as the depth corresponding to the 80% of the SOBP maximum and measured in the distal part, was 29.5 mm in water. The measured dose distribution as well as the LET and dose simulated by using the Geant4 *Hadrontherapy* advanced example that reproduce the entire beamline [28], is reported in Figure 1). The algorithms adopted to compute the LET take into account both primary and secondary particles interacting in a voxel, more details are reported in [27].

Absolute absorbed dose was measured in water, by means of a plane-parallel PTW 34045 advanced-type Markus ionisation chamber, according to the International Atomic Energy Agency Technical Report Series 398 Code of practice [29]. The absorbed dose in water per monitor unit (cGy/M.U.) for the specific SOBP adopted in cell irradiations, was measured at the isocenter at 24 mm depth in water, corresponding to the middle of the SOBP. A reference 25-mm diameter circular collimator was used to determine the beam spot size at the irradiation point. The absolute dose dosimetry was performed just before each irradiation session; the variation of beam calibration on the various experiments amounted to a total of 3%. The overall uncertainty in absolute dose measurement was kept within 1.5%. Details on the irradiation beamlines, dosimetric procedures and related uncertainties for irradiation conditions can be found elsewhere [28]. As regards cell line irradiation, the experimental procedure was described previously [30]. Briefly, cells were seeded in T25 tissue culture flasks with a density of $3\text{--}5 \times 10^5$ cells per flask 24 h before irradiation. T25 were irradiated in the upright position in front of the proton beam exit and hit with separate shots to ensure a complete dose distribution on the flask area. An automatic system for sample positioning and movement was used to move the flasks after each shot in order to cover its entire surface. Cell sample irradiations were carried out positioning each flask at 24 mm, the mid-position of the spread-out Bragg peak, to mimic a clinical condition, with dose values ranging from 1 to 4 Gy and a dose rate of 6 Gy min^{-1} . Finally, the microdosimetric spectra were acquired positioning the mini-TEPC and MicroPlus-Bridge detectors at the entrance and mid position along the same SOBP, while the depths were varied by placing a stack of calibrated PMMA layers between the detectors and the beam collimator [27]. The mini-TEPC is a miniaturized, tissue-equivalent, proportional

counter developed at the Legnaro National Laboratories of the Italian National Institute for Nuclear Physics (INFN-LNL) to work in a sealed mode, without gas flow [25]. The sensitive volume (SV) is a cylinder with both diameter and height of 0.9 mm; the cathode is made of a 0.35 mm-thick A-150 wall, surrounded by a 0.35 mm-thick Rexolite insulator and a 0.2 mm-thick titanium sleeve; the total external diameter is 2.7 mm. The anode is a 10- μm gold plated tungsten wire. The detector was filled with propane gas, at the pressure of 45.4 kPa at 21.8 °C; these conditions simulate a water volume of 1 μm in diameter.

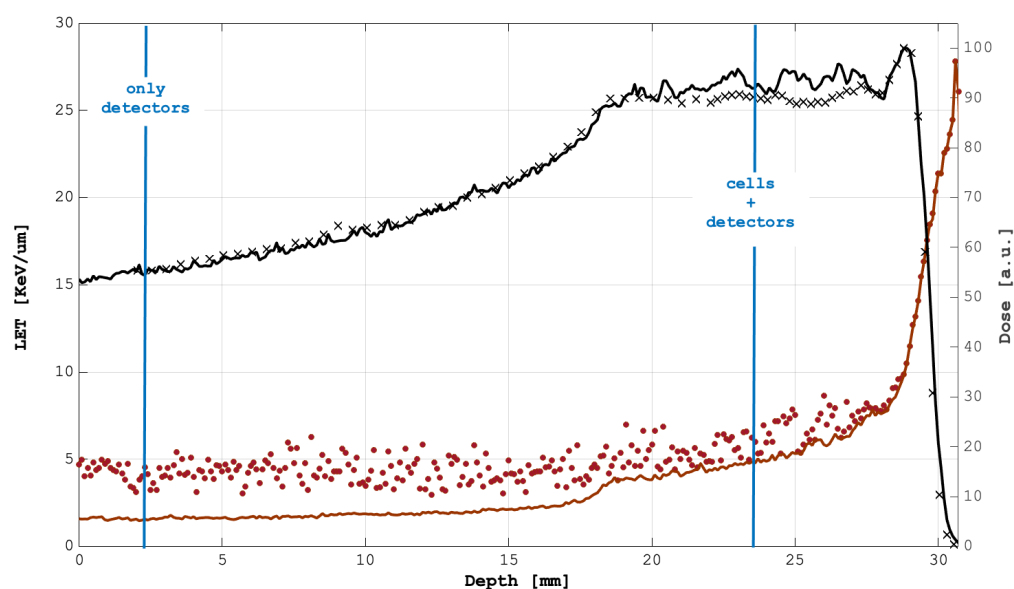


Figure 1. The relative dose measured with the Markus chamber (black crosses), simulated dose distribution (black line), primary LET-dose computed for only primary protons (red line) and LET-Total-dose considering also the contribution of generated secondary particles (red circles) are reported. The vertical blue lines show the positions at which measurements were performed. Simulated and measured values for the absorbed dose are in good agreement when a 2% uncertainty is considered in both sets of data.

The silicon detector adopted was the MicroPlus-Bridge, designed by the Centre for Medical Radiation Physics (CMRP), University of Wollongong, Australia. It consists of an array of 3D right parallelepiped (RPP) shape SVs with an area of $30\ \mu\text{m} \times 30\ \mu\text{m}$ each and a thickness of $10\ \mu\text{m}$, constructed on a silicon-on-insulator wafer. The water equivalent thickness of this microdosimeter is $17.24\ \mu\text{m}$. Additional details and microdosimetric results on the MicroPlus-Bridge microdosimeter technology can be found elsewhere [26]. It has already been shown that the dose mean lineal energy measured with these two detectors reproduces the variation with depth of the dose-averaged LET [23].

2.3. Cell Culture and Clonogenic Assay

The ARPE19 human retinal pigment epithelial cell line was purchased from American Type Culture Collections (ATCC, Manassas, VA, USA) and cultured according to the manufacturer's instructions. Cell culture maintenance was performed with the same methods previously described [31]. The 92.1 human uveal melanoma cell lines were kindly provided by Prof. CD Anfuso and cultured according to the procedure described in the work by Anfuso et collaborators [32]. A clonogenic survival assay was adopted to evaluate cell survival after proton and gamma-ray irradiation. After irradiation, cells were seeded in 6-well plates in triplicate and at an increasing density, depending on the dose delivered; they were incubated for 12–14 days to allow for colony formation. Colonies were stained with 0.05% crystal violet, diluted in 20% ethanol for 30 min at room temperature. Colony-forming ability was determined, both for unirradiated (controls) and irradiated samples, by dividing the counted colony number by the number of cells plated after irradiation

in order to obtain the plating efficiency (PE) and survival fraction (SF) of the samples respectively. For each dose, the SF was then derived by normalizing the above-mentioned results by the PE. For each experimental session, the effect due to the different doses was evaluated on three cell samples. Each point of the survival curves represent the average of three independent experiments. The survival curve was fitted by the linear-quadratic (LQ) equation [33]:

$$S = e^{-\alpha D - \beta D^2} \quad (1)$$

The fit was performed by using the MATLAB-R2019b software, where D is the physical dose deposited by protons and photons, S the surviving fraction, and α and β the radiosensitivity parameters. The fit provided the linear and quadratic parameters with their standard error and the R^2 value. These parameters were used to calculate the enhancement ratios at 10% survival.

Irradiations with γ -rays issued by ^{60}Co source (CIRUS-Cis Biointernational, Gif-sur-Yvette, France) were performed at the Vinca Institute of Nuclear Sciences, Belgrade, Serbia. Cells were irradiated with doses ranging from 1 to 6 Gy at the rate of ≈ 1 Gy/min, in the air at room temperature, following the same experimental procedures as defined for irradiations with protons.

2.4. Microrodosimetric Spectra

The acquired microdosimetric spectra were represented as the distributions of the lineal energy y , the stochastic variable defined as the energy deposited by a single event in a specific volume, divided by the mean chord length [34]. Frequency $f(y)$ and dose $d(y)$ distributions of the lineal energy obey the usual normalization rules of probability distributions:

$$\int_0^{\infty} f(y) dy = 1 \quad (2)$$

and

$$\int_0^{\infty} d(y) dy = 1 \quad (3)$$

with

$$d(y) = \frac{yf(y)}{\int_0^{\infty} yf(y)} \quad (4)$$

The frequency and dose-mean lineal energy values, y_F and y_D , are calculated as:

$$y_F = \int_0^{\infty} yf(y) dy \quad (5)$$

and

$$y_D = \int_0^{\infty} yd(y) dy \quad (6)$$

The microdosimetric lineal energy distribution was used to estimate RBE, following the approach of the biological weighting function [35]. A weighting function $r(y)$ was applied to the measured dose distribution in lineal energy $d(y)$ in order to determine a single parameter, RBE_{μ} , that estimates the biological effectiveness:

$$RBE_{\mu} = \int_0^{\infty} r(y)d(y) dy \quad (7)$$

In this work, the Loncol's function $r(y)$ [36] was adopted to weight the lineal energy. The Loncol's function was numerically determined by an unfolding procedure on empirical and statistical bases. The results of a RBE-microdosimetry intercomparison study between experimental measurements (performed with a TEPC simulating $2 \mu\text{m}$) and in-vivo experimental data of intestinal tolerance assessment by crypt cells regeneration was adopted. The unfolding procedure allowed to determine $r(y)$ by minimizing the differences between biological RBE and RBE_{μ} calculated applying the Equation (7). Despite the function $r(y)$

was derived for a specific biological end-point in vivo (early intestinal tolerance in mice), previous works have already shown that the same function allows to reproduce the trend of the RBE_{10} as a function of depth for a variety of cell lines [22,23]. In this work the RBE_{μ} was here calculated at positions P0 (entrance) and P1 (mid-SOBP). These two results were afterwards multiplied by a constant factor so that RBE_{μ} at position P0 (entrance) equal the clinical value of 1.1:

$$RBE_{\mu}(P_i) = \int_0^{\infty} r(y)d(y, P_i)dy \times [1.1 \div \int_0^{\infty} r(y)d(y, P_0)dy] \quad (8)$$

Applying the LQ model, the estimated RBE_{μ} and the α and β derived from cell survival assessments for reference radiation, were used to calculate α_{μ} , starting from the expression for RBE_{μ} :

$$RBE_{\mu} = \frac{\alpha_{\mu} + \sqrt{\alpha_{\mu}^2 - 4\beta_{\mu} \ln(0.1)}}{\alpha_{\gamma} + \sqrt{\alpha_{\gamma}^2 - 4\beta_{\gamma} \ln(0.1)}} \quad (9)$$

assuming a constant $\beta_{\mu}=\beta_{\gamma}$ and using Equation (9), α_{μ} can be calculated as follows:

$$\alpha_{\mu} = \frac{RBE_{\mu}^2 \cdot A_{\gamma}^2 + 4\beta_{\gamma} \ln(0.1)}{2RBE_{\mu} \cdot A_{\gamma}} \quad (10)$$

with

$$A_{\gamma} = \alpha_{\gamma} + \sqrt{\alpha_{\gamma}^2 - 4\beta_{\gamma} \ln(0.1)} \quad (11)$$

2.5. Monte Carlo Simulations and LEM II Calculations

The RBE values for the two cell lines used in the experimental part of this work were calculated by means of two different approaches. The first was a hybrid procedure, allowing to link the Monte Carlo simulations of the irradiation with a cell-specific look-up table (LUTs) containing the results of the radiation damage calculated with the LEM II model [21]. The LUTs were derived using the software “Survival” [37]. The second approach consisted in the direct use of the Survival code, without including the mixed field contribution, in order to obtain the direct output of the LEM II model. The Monte Carlo simulation of the experimental set-up, including the specific conditions of biological sample irradiation, was carried out using the Geant4 *Hadrontherapy* application [38,39], freely available inside the official Geant4 [40,41] distribution. *Hadrontherapy* simulates the CATANA eye proton therapy beamline with all its beam passive and dynamical transport elements, including the scattering and modulation systems for spatial and energy distribution beam definition, collimators and detectors for the online beamline monitoring. A voxelized detector at the end of the beamline simulates the typical water tank used for the dose curves reconstructions. In order to reproduce the adopted experimental conditions, the tank was divided into slabs perpendicular to the beam propagation direction, along the z-axis. Each slab was $4 \times 4 \times 0.1 \text{ mm}^3$ in dimension. Dose, fluence, dose- and track-averaged LET, survival, RBE and all the related quantities necessary for their estimation were retrieved using the application as described elsewhere [22,27]. Every quantity was stored at the end of each run. A total number of 3.6×10^7 histories were simulated in each simulation; the production cut for secondary protons, gamma and electrons was fixed at 0.1 mm. All calculations were carried out using the 10.07.p01 version of Geant4.

3. Results and Discussion

One of the aims of this work is the comparison of three methods to calculate the RBE in a clinical setting: microdosimetric-based, Monte Carlo and LEM II model. All of the proposed approaches were compared with experimental data. Radiation-induced cell death was measured by clonogenic assay and RBE values were calculated using the Linear-Quadratic model. The clonogenic survival curves of two specific cell lines were

experimentally measured at 24 mm, the mid-position of the 62 MeV clinical proton SOBP. Additionally, at the SOBP entrance, the survival curves were also estimated from the experimental measurements of the microdosimetric spectra. The estimation of the survival curves with these three approaches permitted the estimation of the RBE values in the centre of the SOBP region. The radiobiological effects of protons were experimentally evaluated using the human 92.1 uveal melanoma cell line. In order to evaluate the damage induced by proton therapy in a typical tissue belonging to the same anatomical site, the human normal retinal pigment epithelial ARPE-19 cell line was also irradiated. The assessment of the detrimental effects in healthy tissues due to radiotherapy is pivotal, especially for the treatment of cancers affecting the eye since even slight impairment of the normal ocular tissue would lead to a loss of function of the entire organ [42]. The results of the clonogenic curves with the fitted parameters, for the two cell lines irradiated at the proton mid-SOBP and under a reference gamma beam, are summarised in Table 1. Table also report the corresponding derived values of RBEs.

Table 1. Survival curve parameters measured for proton and gamma irradiation of the 92.1 and ARPE-19 cell line. The statistical parameters of the double exponential fit function and the values of the derived RBEs are reported.

	Irr. Type	$\alpha(\text{Gy}^{-1})$	$\beta(\text{Gy}^{-2})$	α/β	Fit. Std. Err.	RBE_{10}
92.1	γ -rays	0.20 ± 0.03	0.076 ± 0.004	2.68	0.02	1.4
	protons	0.40 ± 0.02	0.095 ± 0.003	4.25	0.007	
ARPE19	γ -rays	0.34 ± 0.14	0.03 ± 0.02	11.33	0.02	1.2
	protons	0.43 ± 0.01	0.041 ± 0.003	10.49	0.04	

Two fundamental radiobiological parameters were contextually obtained, the alpha and beta values, together with their ratio. Within the LQ model context, the alpha and beta coefficients of the clonogenic survival curves represent the single-hit, lethal damage, generally not repairable, and the multiple-hit damage, associated with sub lethal damage, respectively. Sublethal damage is responsible for the shouldered part of the clonogenic curve and can be usually repaired [43]. The α/β ratio is a useful indicator of radiosensitivity, hence, its calculation is of paramount importance to evaluate the cell response to the radiation therapy (RT) treatment [44,45]. The clonogenic endpoint has, in fact, shown a lower radiosensitivity exhibited by the ocular cancer cells with respect to the normal cells as expected. In addition, for both cell lines, an increased RBE with proton beam irradiation was obtained. The capability of the two microdosimeters to describe not only the RBE but also the survival curve at the mid-SOBP was then investigated. Figure 2 shows the acquired microdosimetric spectra from which the RBEs values and the parameters of the corresponding clonogenic curves were derived. Distributions are presented as $y d(y)$ versus y on a logarithmic x -axis to facilitate visual interpretation. In this representation, the area under the curve between two values of y is proportional to the fraction of physical absorbed dose due to the events in that interval.

Specifically, in Figure 2 the two positions (entrance and mid of the SOBP) and the two detectors (mini-TEPC and MicroPlus Bridge) are considered. In the same figures, the Loncol's biological weighting function $r(y)$ and the corresponding weighted-dose curves $yr(y)d(y)$ are also reported. The observed increase of the area under the red curve (i.e., the $yr(y)d(y)$ curve) for the spectra acquired at the cell position (bottom row of Figure 2), reflects an increase in the RBE. It can be observed, in fact, that at the entrance position the biologically weighted distributions overlap almost perfectly with the un-weighted distributions, because for $y < 10 \text{ keV}/\mu\text{m}$ the weighting function $r(y)$ almost equals almost equals 1. Different behaviour can be observed at the mid-SOBP, where the weighting function augments the contribution of events above $10 \text{ keV}/\mu\text{m}$ leading to an increase of the RBE_{μ} (Equations (8)–(11)). The RBE calculated at the mid-SOBP with the mini-TEPC, ($RBE_{\mu}\text{-TECP} = 1.18$), resulted slightly higher than that calculated with the Microplus

Bridge (RBE_{μ} -MicroPlus = 1.12). With respect to the entrance position, the RBE_{μ} -TEPC at the mid-SOBP increases by about 17%, and the RBE_{μ} -MicroPlus increases by about 13%. The reason for this underestimation of the MicroPlus with respect to the TEPC is the larger simulated site size (about 17 μm with respect to 1 μm of the TEPC): low energy protons stop inside the silicon thickness, therefore the largest proton events (proton-edge) are at about 40 keV/ μm for the Microplus, while they are at about 140 keV/ μm for the mini-TEPC. The RBE_{μ} values, corrected by a constant factor to have $RBE_{\mu} = 1.1$ at the entrance position of the SOBPs, and the linear parameters α_{μ} of the linear-quadratic model, calculated using Equation (11), are reported in Table 2. The β_{μ} was assumed to be equal to β_{γ} (see Section 2.4).

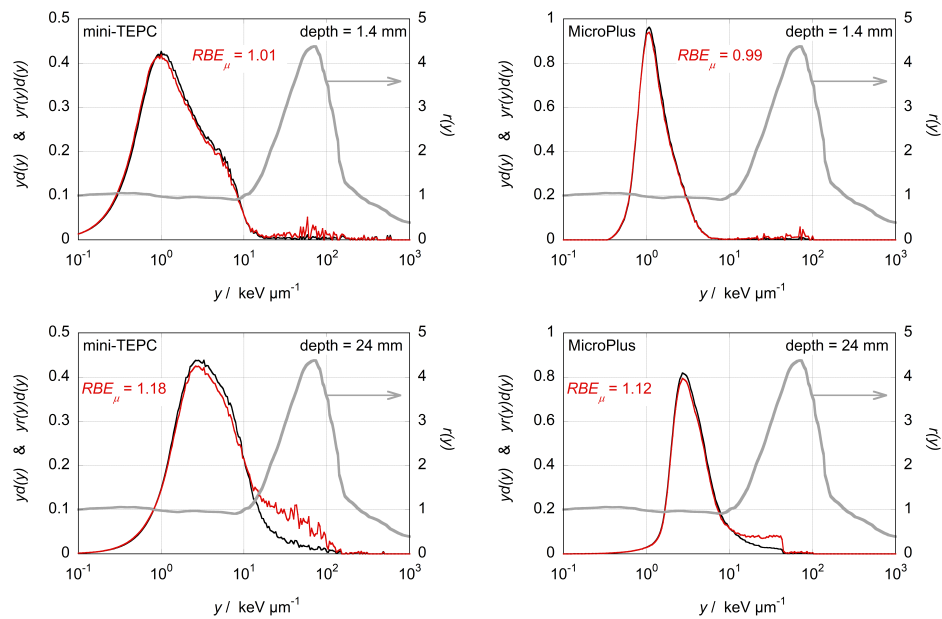


Figure 2. The microdosimetric spectra $yd(y)$ measured at the entrance (**top**) and at cell position (**bottom**) acquired with the mini-TEPC (**left**) and with the MicroPlus Bridge microdosimeter (**right**). The thick grey line represents the biological weighting function $r(y)$ (Loncol, 1994). The red curves are the weighted distributions $yr(y)d(y)$. The black curves are the experimental microdosimetric spectra. See text for more details.

Table 2. RBE_{μ} calculated from microdosimetric spectra, and corrected by a constant factor to have $RBE_{\mu} = 1.1$ in entrance. The parameters α_{μ} TEPC and α_{μ} MicroPlus were calculated with Equations (8)–(11).

Cell Type	RBE_{μ} -TEPC	RBE_{μ} -MicroPlus	α_{μ} TEPC	α_{μ} MicroPlus
92.1	1.29	1.24	0.35 ± 0.03	0.31 ± 0.02
ARPE19	1.29	1.24	0.45 ± 0.04	0.41 ± 0.04

Finally, the survival curves relative to the mid-SOBP position and derived from the microdosimetric data, experimentally measured from cell irradiation experiments and calculated with the described Monte Carlo and using the Survival software [37], are reported in Figure 3 (92.1 cell line) and Figure 4 (ARPE-19 cell line). Both figures also show the survival curve measured for the ^{60}Co gamma-ray irradiation. The survival experimental curves were fitted using the double exponential function (Equation (1)) and the α and β derived from it were reported in Table 1. The survival fraction related to the experimental data and applied approaches for the two investigated curves is reported in the Table 3 (92.1 cell line) and Table 4 ARPE-19 cell line).

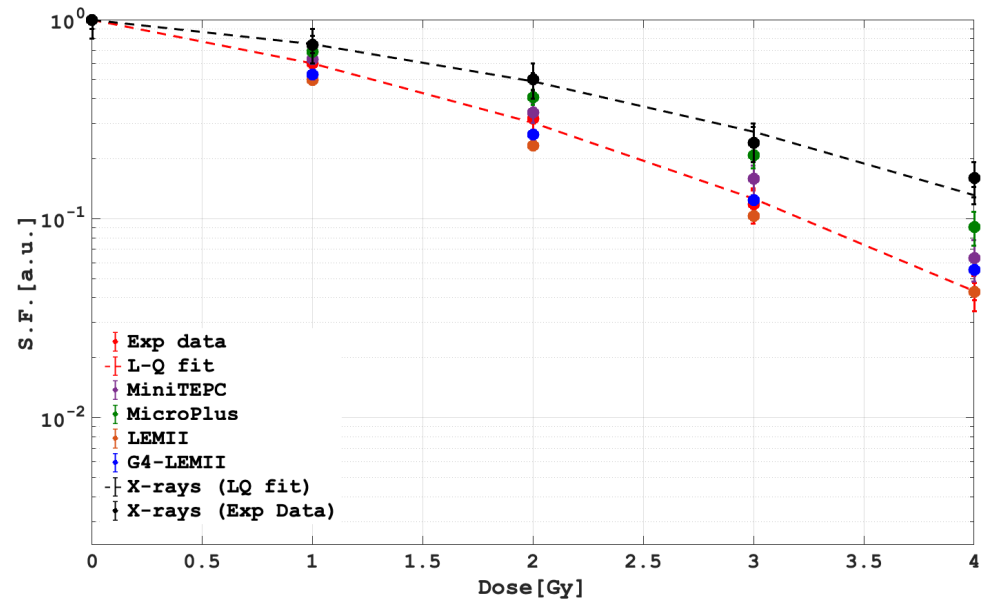


Figure 3. Survival fractions for 92.1. Biological survival data acquired with proton beam irradiations (red symbols) are plotted together with the linear-quadratic best fit (red dashed line). Biological survival data acquired with gamma rays (black symbols) are plotted together with the best fit (black dashed line). The survival fractions predicted from microdosimetric measurements calibrated on gamma-rays cell survival are also plotted. Purple and green points are related to the mini-TEPC and MicroPlus respectively. The blue points were calculated by coupling the Monte Carlo Geant4 with the LEM-II model. Finally, the orange points are obtained with the LEM-II module.

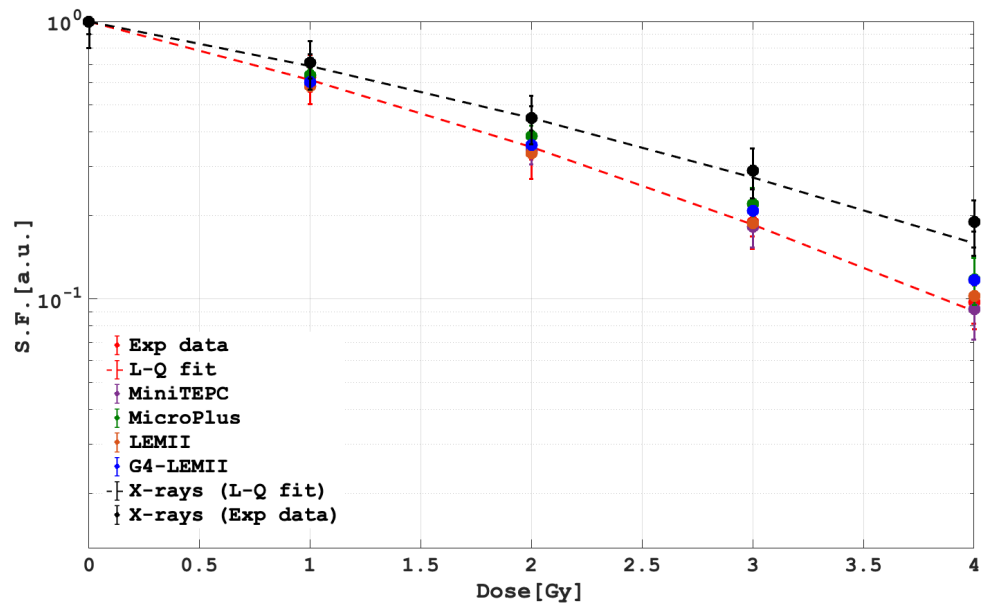


Figure 4. Survival fractions for ARPE19. Biological survival data acquired with proton beam irradiations (red symbols) are plotted together with the linear-quadratic best fit (red dashed line). Biological survival data acquired with gamma rays (black symbols) are plotted together with the best fit (black dashed line). The survival fractions predicted from microdosimetric measurements calibrated on gamma-rays cell survival are also plotted. Purple and green points are related to the mini-TEPC and MicroPlus respectively. The blue points were calculated by coupling the Monte Carlo Geant4 with the LEM-II model. Finally, the orange points are obtained with the LEM-II module.

Table 3. Survival Fraction of the 92.1 cell line obtained applying the three approaches: LEMII, Geant4 coupled with LEMII and Loncol's function applied to the microdosimetric spectra. The first column reports experimental data.

Dose [Gy]	Exp Data	LEMII	G4-LEMII	mini-TEPC	MicroPlus
1	0.606 ± 0.121	0.496 ± 0.009	0.528 ± 0.011	0.62 ± 0.03	0.68 ± 0.02
2	0.304 ± 0.061	0.232 ± 0.004	0.263 ± 0.005	0.34 ± 0.03	0.41 ± 0.02
3	0.126 ± 0.025	0.102 ± 0.002	0.124 ± 0.002	0.15 ± 0.02	0.03 ± 0.20
4	0.043 ± 0.008	0.042 ± 0.001	0.055 ± 0.001	0.06 ± 0.01	0.09 ± 0.01

Table 4. Survival Fraction of the ARPE19 cell line obtained applying the three approaches: LEMII, Geant4 coupled with LEMII and Loncol's function applied to the microdosimetric spectra. The first column reports experimental data.

Dose [Gy]	Exp Data	LEMII	G4-LEMII	mini-TEPC	MicroPlus
1	0.618 ± 0.123	0.584 ± 0.011	0.605 ± 0.012	0.60 ± 0.03	0.64 ± 0.02
2	0.353 ± 0.071	0.334 ± 0.006	0.358 ± 0.007	0.34 ± 0.03	0.38 ± 0.03
3	0.186 ± 0.037	0.187 ± 0.003	0.207 ± 0.004	0.18 ± 0.02	0.22 ± 0.03
4	0.091 ± 0.018	0.102 ± 0.002	0.117 ± 0.002	0.09 ± 0.01	0.11 ± 0.02

The agreement between the three investigated methods, with the experimental radiobiological data, was statistically evaluated by applying the χ^2 test. Results of the test (p -values included) are reported in Tables 5 and 6: the χ^2 values are calculated taking into account the data reported in the Tables 3 and 4.

Table 5. Results of the χ^2 test for the comparison of the experimental survival curves of 92.1 cells against the survival fraction calculated with the LEM II, Geant4 coupled with LEM II and the Loncol's function applied with the microdosimetric spectra obtained with the two detectors. The corresponding χ^2 probabilities are calculated for four degrees of freedom.

92.1		
	χ^2	p -Value
LEM2	3.06	0.38
LEM2-G4	2.70	0.44
MicroPlus	12.87	0.004
MiniTEPC	2.34	0.50

Table 6. Results of the χ^2 test for the comparison of the experimental survival curves of ARPE19 cells against the survival fraction calculated with the LEM II, Geant4 coupled with LEM II and the Loncol's function applied with the microdosimetric spectra obtained with the two detectors. The corresponding χ^2 probabilities are calculated for four degrees of freedom.

ARPE19		
	χ^2	p -Value
LEM2	0.54	0.91
LEM2-G4	2.42	0.49
MicroPlus	1.56	0.67
MiniTEPC	0.04	0.99

In almost all the investigated cases, the resulting p -value is well above 0.25, showing that the models are able to well reproduce the experimental data. The p -value calculated applying the Loncol's function and using the microdosimetric spectra measured with the

MicroPlus probe is lower than 0.05 as shown in Table 5. This disagreement could be related to the higher sensitive volume of the adopted detector with respect to Mini-TEPC.

4. Conclusions and Perspectives

In this study, we showed that the LEM-II model, the Monte Carlo-based LEM model and a semi-empirical method based on microdosimetric spectra, can adequately reproduce experimentally derived survival curves from *in vitro* cell irradiations performed at the mid-SOBP of the CATANA 62 MeV clinical proton beam.

For both cell lines, an RBE greater than 1.1 was measured and reproduced applying all of the investigated approaches. This points out that the biological damage of both healthy and tumorigenic cells is underestimated if a fixed RBE of 1.1 is assumed. Microdosimetric spectra were measured at the entrance and mid-SOBP position with both a mini-TEPC, simulating a 1 μm water site size, and the MicroPlus microdosimeter (17 μm water equivalent thickness). Despite the markedly different microdosimetric spectra obtained with these two detectors, when the Loncol's weighting function is applied to the dose distributions both lead to an assessment of the RBE10 that is in good agreement with radiobiological data for ARPE-19 cells obtained in the same beamline. The higher discrepancy obtained with the 92.1 cell line and the solid-state detector could be due to a lower detector sensitivity related to the higher SV volume. The remarkable obtained result showed the potentiality of using a microdosimetric spectrum to predict not only the RBE but also the full survival curve, at least at the mid-position of the 62 MeV proton SOBPs. Currently, different commercial treatment planning softwares for proton therapy incorporate tools for calculating LET distributions and RBE prediction. However, while the dose prescriptions calculated by the treatment planning are routinely verified with certified ionization chambers, there is no commercial equipment currently available to perform routine verification of LET or RBE distributions calculated by the TPS. The Local Effect Model is the computational radiobiological approach most widely used in hadrontherapy. The LEM model was fully integrated into the analytical treatment planning system TRiP98 and successfully tested for clinical application. In this work, the good agreement between the Monte-Carlo-based LEM model and LEM-II model with the experimental data clearly evidence how a TPS based on an RBE and LET prediction could improve the estimation of the radiobiological response of the treated neoplasia as well as the surrounding healthy tissues. Moreover, the pretty good accordance between the semi-empirical methods based on microdosimetric spectra with the experimental data shows that the LET estimation procedure should be successfully inserted in the clinical routine to optimize the RBE distribution. The current study identifies a clinical and critical aspect of the uveal melanoma protontherapy treatment. The correct evaluation of the damage induced by ionizing radiation during RT treatment, also thanks to Monte Carlo-based simulations, represents a valuable and potent tool to foresee the impact of ionizing radiation on cancer tissues. Moreover, studying both healthy and tumorigenic cells allows obtaining fundamental information about the biological effects induced by an erroneous dose distribution during a proton therapy ocular treatment plan. The biological response is therefore of paramount importance to provide an estimate of the possible adverse effects deriving by beam forward straggling. A correct prediction of the damage is a key point for a more personalized TPS.

Author Contributions: M.C., F.P.C., V.B., L.M. (Luigi Minafra) carried out cell survival measurements at INFN-LNS. A.R.F., I.P., V.P., O.K. performed the cell survival measurements with gamma rays. L.M. (Lorenzo Manti), P.B., S.R., G.R., G.I.F., G.P., G.C., G.A.P.C., V.C. provided overall conceptual contribution. G.A.P.C. and G.P. supervised beam dosimetry at INFN-LNS. V.C., G.P., G.A.P.C. performed microdosimetric measurements. V.C. estimated the biological damage starting from microdosimetric spectra. G.P. performed the Monte Carlo simulations. G.P. conceptualized the study and wrote the first draft of the manuscript. All authors have read and agreed to the published version of the manuscript.

Funding: The authors wish to acknowledge financial support from MAECI PGR No. 00794 Italy-Serbia Project and from the Ministry of Education, Science and Technological Development of Serbia. L.Minafra was supported by the Short Term Mobility (STM) Program (Bando 2018, Consiglio Nazionale delle Ricerche-CNR, Italy). This work was also supported by European Structural and Investment Fund and the Czech Ministry of Education, Youth and Sports (Project International mobility MSCA-IF IV FZU-CZ.02.2.69/0.0/0.0/20-079/0017754).

Institutional Review Board Statement: Each involved institute was informed about the work done.

Informed Consent Statement: Informed consent is not applicable.

Data Availability Statement: Data are not publicly available.

Conflicts of Interest: The authors declare that this device is protected by a national and International patent and that it could be commercialised in the future. At the moment of writing the described device is not commercialised and no conflict of interest is present.

References

1. Liu, H.; Chang, J.Y. Proton therapy in clinical practice. *Chin. J. Cancer* **2011**, *30*, 315–326. [[CrossRef](#)] [[PubMed](#)]
2. Lühr, A.; von Neubeck, C.; Krause, M.; Troost, E.G.C. Relative biological effectiveness in proton beam therapy—Current knowledge and future challenges. *Clin. Transl. Radiat. Oncol.* **2018**, *9*, 35–41. [[CrossRef](#)]
3. Underwood, T.S.; McMahon, S.J. Proton relative biological effectiveness (RBE): A multiscale problem. *Br. J. Radiol.* **2019**, *92*, 20180004. [[CrossRef](#)] [[PubMed](#)]
4. Giovannini, G.; Böhlen, T.; Cabal, G.; Bauer, J.; Tessonier, T.; Frey, K.; Debus, J.; Mairani, A.; Parodi, K. Variable RBE in proton therapy: Comparison of different model predictions and their influence on clinical-like scenarios. *Radiat. Oncol.* **2016**, *11*, 2718503. [[CrossRef](#)] [[PubMed](#)]
5. Paganetti, H. Relating the proton relative biological effectiveness to tumor control and normal tissue complication probabilities assuming interpatient variability in α/β . *Acta Oncol.* **2017**, *56*, 1379–1386. [[CrossRef](#)] [[PubMed](#)]
6. Chaudhary, P.; Marshall, T.; Manti, L.; Currell, F.J.; McMahon, S.J.; Kavanagh, J.N.; Cirrone, G.A.P.; Romano, F.; Prise, K.M.; Schettino, G. Relative Biological Effectiveness variation along monoenergetic and modulated Bragg peaks of a 62 MeV therapeutic proton beam: A pre-clinical assessment. *Int. J. Radiat. Oncol. Biol. Phys.* **2014**, *90*, 27–35. [[CrossRef](#)]
7. Cuaron, J.J.; Chang, C.; Lovelock, M.; Higginson, D.S.; Mah, D.; Cahlon, O.; Powell, S. Exponential Increase in Relative Biological Effectiveness Along Distal Edge of a Proton Bragg Peak as Measured by Deoxyribonucleic Acid Double-Strand Breaks. *Int. J. Radiat. Oncol. Biol. Phys.* **2016**, *95*, 62–69. [[CrossRef](#)]
8. Willers, H.; Allen, A.; Grosshans, D.; McMahon, S.J.; von Neubeck, C.; Wiese, C.; Vikram, B. Toward A variable RBE for proton beam therapy. *Radiother. Oncol.* **2018**, *42*, 128, 68–75. [[CrossRef](#)]
9. Vitti, E.T.; Parsons, J.L. The Radiobiological Effects of Proton Beam Therapy: Impact on DNA Damage and Repair. *Cancers* **2019**, *11*, 946. [[CrossRef](#)] [[PubMed](#)]
10. Vanderwaeren, L.; Dok, R.; Verstrepen, K.; Nuyts, S. Clinical Progress in Proton Radiotherapy: Biological Unknowns. *Cancers* **2021**, *13*, 604. [[CrossRef](#)]
11. Friedrich, T.; Scholz, U.; Elsässer, T.; Durante, M.; Scholz, M. Systematic analysis of RBE and related quantities using a database of cell survival experiments with ion beam irradiation. *J. Radiat. Res.* **2013**, *54*, 494–514. [[CrossRef](#)]
12. Keshazare, S.; Masoudi, S.F.; Rasouli, F.S. Effects of defining realistic compositions of the ocular melanoma on proton therapy. *J. Biomed. Phys. Eng.* **2014**, *4*, 141–150. [[PubMed](#)]
13. Verma, V.; Mehta, M.P. Clinical Outcomes of Proton Radiotherapy for Uveal Melanoma. *Clin. Oncol. (R. Coll. Radiol.)* **2016**, *28*, e17–e27. [[CrossRef](#)] [[PubMed](#)]
14. Mishra, K.K.; Daftari, I.K. Proton therapy for the management of uveal melanoma and other ocular tumors. *Chin. Clin. Oncol.* **2016**, *5*, 50 [[CrossRef](#)] [[PubMed](#)]
15. Spatola, C.; Liardo, R.L.E.; Milazzotto, R.; Raffaele, L.; Salamone, V.; Basile, A.; Foti, P.V.; Palmucci, S.; Cirrone, G.A.P.; Cuttone, G.; et al. Radiotherapy of Conjunctival Melanoma: Role and Challenges of Brachytherapy. *Appl. Sci.* **2020**, *10*, 9071. [[CrossRef](#)]
16. Messineo, D.; Barile, G.; Morrone, S.; La Torre, G.; Turchetti, P.; Accetta, L.; Trovato Battagliola, E.; Agostinelli, E.; Pacella, F. Meta-analysis on the utility of radiotherapy for the treatment of Ocular Melanoma. *Clin. Ther.* **2020**, *170*, e89–e98.
17. Courdi, A.; Brassart, N.; Héroult, J.; Chauvel, P. The depth-dependent radiation response of human melanoma cells exposed to 65 MeV protons. *Br. J. Radiol.* **1994**, *67*, 800–804. [[CrossRef](#)]
18. Petrović, I.; Ristić-Fira, A.; Todorović, D.; Korićanac, L.; Valastro, L.; Cirrone, P.; Cuttone, G. Response of a radioresistant human melanoma cell line along the proton spread-out Bragg peak. *Int. J. Radiat. Biol.* **2010**, *86*, 742–751. [[CrossRef](#)]
19. Petrović, I.M.; Ristić Fira, A.M.; Keta, O.D.; Petković, V.D.; Petringa, G.; Cirrone, P.; Cuttone, G. A radiobiological study of carbon ions of different linear energy transfer in resistant human malignant cell lines. *Int. J. Radiat. Biol.* **2020**, *96*, 1400–1412. [[CrossRef](#)]
20. Jasińska-Konior, K.; Pochylczuk, K.; Czajka, E.; Michalik, M.; Romanowska-Dixon, B.; Swakoń, J.; Urbańska, K.; Elas, M. Proton beam irradiation inhibits the migration of melanoma cells. *PLoS ONE* **2017**, *12*, e0186002.

21. Scholz, M.; Kellerer, A.M.; Kraft-Weyrather, W.; Kraft, G. Computation of cell survival in heavy ion beams for therapy. The model and its approximation. *Radiat. Environ. Biophys.* **1997**, *36*, 59–66. [[CrossRef](#)] [[PubMed](#)]
22. Petringa, G.; Romano, F.; Manti, L.; Pandola, L.; Attili, A.; Cammarata, F.; Cuttone, G.; Forte, G.; Manganaro, L.; Pipek, J.; et al. Radiobiological quantities in proton-therapy: Estimation and validation using Geant4-based Monte Carlo simulations. *Phys. Med.* **2019**, *58*, 72–80. [[CrossRef](#)] [[PubMed](#)]
23. Conte, V.; Agosteo, S.; Bianchi, A.; Bolst, D.; Bortot, D.; Catalano, R.; Cirrone, G.A.P.; Colautti, P.; Cuttone, G.; Guatelli, S.; et al. Microdosimetry of a therapeutic proton beam with a mini-TEPC and a MicroPlus-Bridge detector for RBE assessment. *Phys. Med. Biol.* **2020**, *65*, 245018. [[CrossRef](#)]
24. De Nardo, L.; Cesari, V.; Donà, G.; Magrin, G.; Colautti, P.; Conte, V.; Tornielli, G. Mini-TEPCs for radiation therapy. *Radiat. Prot. Dosim.* **2004**, *108*, 345–352. [[CrossRef](#)] [[PubMed](#)]
25. Conte, V.; Bianchi, A.; Selva, A.; Petringa, G.; Cirrone, G.A.P.; Parisi, A.; Vanhavere, F.; Colautti, P. Microdosimetry at the CATANA 62 MeV proton beam with a sealed miniaturized TEPC. *Phys. Med.* **2020**, *64*, 114–122. [[CrossRef](#)] [[PubMed](#)]
26. Rosenfeld, A.B. Novel detectors for silicon based microdosimetry, their concepts and applications. *Nucl. Instrum. Methods Phys. Res. Sect. Accel. Spectrometers Detect. Assoc. Equip.* **2016**, *809*, 156–170. [[CrossRef](#)]
27. Petringa, G.; Pandola, L.; Agosteo, S.; Catalano, R.; Colautti, P.; Conte, V.; Cuttone, G.; Fan, K.; Mei, Z.; Rosenfeld, A.B.; et al. Monte Carlo implementation of new algorithms for the averaged-dose and -track linear energy transfer evaluation in 62 MeV clinical proton beams. *Phys. Med. Biol.* **2020**, *65*, 235043. [[CrossRef](#)]
28. Cirrone, G.A.; Cuttone, G.; Raffaele, L.; Salamone, V.; Avitabile, T.; Privitera, G.; Spatola, C.; Amico, A.G.; Larosa, G.; Leanza, R.; et al. Clinical and Research Activities at the CATANA Facility of INFN-LNS: From the Conventional Hadrontherapy to the Laser-Driven Approach. *Front. Oncol.* **2017**, *7*, 223. [[CrossRef](#)]
29. Development of procedures for in vivo dosimetry in radiotherapy. In *Technical Report Series n. 8*; International Atomic Energy Agency: Wien, Austria, 2013.
30. Bravatà, V.; Cammarata, F.P.; Minafra, L.; Pisciotta, P.; Scazzone, C.; Manti, L.; Savoca, G.; Petringa, G.; Cirrone, G.A.P.; Cuttone, G.; et al. Proton-irradiated breast cells: Molecular points of view. *J. Radiat. Res.* **2019**, *60*, 451–465. [[CrossRef](#)]
31. Cammarata, F.P.; Torrisi, F.; Forte, G.I.; Minafra, L.; Bravatà, V.; Pisciotta, P.; Savoca, G.; Calvaruso, M.; Petringa, G.; Cirrone, G.A.P.; et al. Proton Therapy and Src Family Kinase Inhibitor Combined Treatments on U87 Human Glioblastoma Multiforme Cell Line. *Int. J. Mol. Sci.* **2019**, *20*, 4745. [[CrossRef](#)]
32. Anfusio, C.D.; Longo, A.; Distefano, A.; Amorini, A.M.; Salmeri, M.; Zanghi, G.; Giallongo, C.; Giurdanella, G.; Lupo, G. Uveal Melanoma Cells Elicit Retinal Pericyte Phenotypical and Biochemical Changes in an in Vitro Model of Coculture. *Int. J. Mol. Sci.* **2020**, *21*, 5557. [[CrossRef](#)] [[PubMed](#)]
33. Franken, N.; Rodermond, H.; Stap, J.; Haveman, J.; Bree, C. Clonogenic assay of cells in vitro. *Nat. Protocols* **2006**, *1*, 2315–2319. [[CrossRef](#)]
34. Menzel, H.G. International Commission on Radiation Units and Measurements. *J. Int. Comm. Radiat. Units Meas.* **2014**, *14*, 1–2.
35. Paganetti, H.; Olko, P.; Kobus, H.; Becker, R. Calculation of relative biological effectiveness for proton beams using biological weighting functions. *Int. J. Radiat. Oncol. Biol. Phys.* **1997**, *37*, 719–729. [[CrossRef](#)]
36. Loncol, T.; Cosgrove, V.; Denis, J.M.; Gueulette, J.; Mazal, A.; Menzel, H.G.; Pihet, P.; Sabattier, R. Radiobiological Effectiveness of Radiation Beams with Broad LET Spectra: Microdosimetric Analysis Using Biological Weighting Functions. *Radiat. Prot. Dosim.* **1994**, *52*, 347–352. [[CrossRef](#)]
37. Manganaro, L.; Russo, G.; Bourhaleb, F.; Fausti, F.; Giordanengo, S.; Monaco, V.; Sacchi, R.; Vignati, A.; Cirio, R.; Attili, A. Survival: A simulation toolkit introducing a modular approach for radiobiological evaluations in ion beam therapy. *Phys. Med. Biol.* **2018**, *63*, 08NT01. [[CrossRef](#)] [[PubMed](#)]
38. Cirrone, G.P.; Cuttone, G.; Guatelli, S.; Nigro, S.L.; Mascialino, B.; Pia, M.G.; Raffaele, L.; Russo, G.; Sabini, M.G. Implementation of a new Monte Carlo GEANT4 simulation tool for the development of a proton therapy beam line and verification of the related dose distributions. *IEEE Trans. Nucl. Sci.* **2005**, *52*, 1756–1758. [[CrossRef](#)]
39. Cirrone, G.A.P.; Cuttone, G.; Mazzaglia, E.S.; Romano, F.; Sardina, D.; Agodi, C.; Attili, A.; Blancato, A.A.; De Napoli, M.; Di Rosa, F.; et al. Hadrontherapy: A 4-based tool for proton/ion-therapy studies. *Prog. Nucl. Sci. Technol.* **2011**, *2*, 207–212. [[CrossRef](#)]
40. Allison, J.; Amako, K.; Apostolakis, J.; Arce, P.; Asai, M.; Aso, T.; Bagli, E.; Bagulya, A.; Banerjee, S.; Barrand, G.J.N.I.; et al. Recent Developments in Geant4. *Nucl. Instrum. Methods* **2016**, *835*, 186–225. [[CrossRef](#)]
41. Allison, J.; Amako, K.; Apostolakis, J.E.A.; Araujo, H.A.A.H.; Dubois, P.A.; Asai, M.A.A.M.; Barrand, G.A.B.G.; Capra, R.A.C.R.; Chauvie, S.A.C.S.; Chytrcek, R.A.C.R.; et al. Geant4 Developments and Applications. *IEEE Trans. Nucl. Sci.* **2006**, *53*, 270–278. [[CrossRef](#)]
42. Calipel, A.; Lux, A.L.; Guérin, S.; Lefaix, J.L.; Laurent, C.; Bernaudin, M.; Mouriaux, F. Geant4 Developments and Applications. *Investig. Ophthalmol. Vis. Sci.* **2015**, *56*, 3085–3094. [[CrossRef](#)]
43. McMahon, S.J. The linear quadratic model: Usage, interpretation and challenges. *Phys. Med. Biol.* **2019**, *64*, 01TR01. [[CrossRef](#)] [[PubMed](#)]

-
44. Savoca, G.; Calvaruso, M.; Minafra, L.; Bravatà, V.; Cammarata, F.P.; Iacoviello, G.; Abbate, B.; Evangelista, G.; Spada, M.; Forte, G.I.; et al. Local Disease-Free Survival Rate (LSR) Application to Personalize Radiation Therapy Treatments in Breast Cancer Models. *J. Pers. Med.* **2020**, *10*, 177. [[CrossRef](#)] [[PubMed](#)]
 45. Williams, M.V.; Denekamp, J.; Fowler, J.F. A review of alpha/beta ratios for experimental tumors: Implications for clinical studies of altered fractionation. *Int. J. Radiat. Oncol. Biol. Phys.* **1985**, *11*, 87–96. [[CrossRef](#)]